Journal of Experimental Botany, Vol. 63, No. 15, pp. 5645–5658, 2012
doi:10.1093/jxb/ers218

Journal of Experimental Botany
www.jxb.oxfordjournals.org

RESEARCH PAPER

Phylogeny and photosynthetic pathway distribution in *Anticharis* Endl. (Scrophulariaceae)

Roxana Khoshravesh[1], Hossein Akhani[1,*], Tammy L. Sage[2], Bertil Nordenstam[3] and Rowan F. Sage[2]

[1] Department of Plant Sciences, School of Biology, College of Sciences, University of Tehran, PO Box 14155–6455, Tehran, Iran
[2] Department of Ecology and Evolutionary Biology, University of Toronto, 25 Willcocks Street, Toronto, Ontario M5S 3B2, Canada
[3] Department of Phanerogamic Botany, Swedish Museum of Natural History, PO Box 50007, S-10405 Stockholm, Sweden

* To whom correspondence should be addressed. E-mail: akhani@khayam.ut.ac.ir

Received 12 April 2012; Revised 22 June 2012; Accepted 9 July 2012

Abstract

C_4 photosynthesis independently evolved >62 times, with the majority of origins within 16 dicot families. One origin occurs in the poorly studied genus *Anticharis* Endl. (Scrophulariaceae), which consists of ~10 species from arid regions of Africa and southwest Asia. Here, the photosynthetic pathway of 10 *Anticharis* species and one species from each of the sister genera *Aptosimum* and *Peliostomum* was identified using carbon isotope ratios ($\delta^{13}C$). The photosynthetic pathway was then mapped onto an internal transcribed spacer (ITS) phylogeny of *Anticharis* and its sister genera. Leaf anatomy was examined for nine *Anticharis* species and plants from *Aptosimum* and *Peliostomum*. Leaf ultrastructure, gas exchange, and enzyme distributions were assessed in *Anticharis glandulosa* collected in SE Iran. The results demonstrate that C_3 photosynthesis is the ancestral condition, with C_4 photosynthesis occurring in one clade containing four species. C_4 *Anticharis* species exhibit the atriplicoid type of C_4 leaf anatomy and the NAD-malic enzyme biochemical subtype. Six *Anticharis* species had C_3 or C_3–C_4 $\delta^{13}C$ values and branched at phylogenetic nodes that were sister to the C_4 clade. The rest of *Anticharis* species had enlarged bundle sheath cells, close vein spacing, and clusters of chloroplasts along the centripetal (inner) bundle sheath walls. These traits indicate that basal-branching *Anticharis* species are evolutionary intermediates between the C_3 and C_4 conditions. *Anticharis* appears to be an important new group in which to study the dynamics of C_4 evolution.

Key words: C_3–C_4 intermediates, Kranz anatomy, Lamiales, phylogeny.

Introduction

The C_4 photosynthetic pathway is one of the most convergent complex evolutionary phenomena in the living world. Over 62 evolutionary origins of the C_4 pathway have been identified in 19 families of angiosperms (R.F. Sage *et al*., 2011; Sage *et al*., 2012). These origins tend to cluster in certain taxonomic groups, notably the Caryophyllales (Chenopods, Amaranths, and assorted arid-zone genera such as *Portulaca* and *Boerhavia*) and Poales (Grasses and Sedges) (Christin *et al*., 2011; R.F. Sage *et al*., 2011). In a few taxonomic orders, C_4 photosynthesis has originated once or twice, and occurs in isolation from the clustered origins in groups such as the grasses and chenopods. One of these orders, the Lamiales, has given rise to two distinct lineages of C_4 photosynthesis, one in the genus *Blepharis* (Acanthaceae) and the other in *Anticharis* (Scrophulariaceae) (Akhani *et al*., 2008; R.F. Sage *et al*., 2011). *Anticharis* is notable for a number of reasons. It contains the only known C_4 species in the Scrophulariaceae s.l., a large and diverse family with hundreds of genera and thousands of species (Sage and Monson, 1999; Schäferhoff *et al*., 2010; Plant List, 2012). It is a small, poorly studied genus with 8–12 species (Plant List, 2012). One species, *Anticharis senegalensis*, exhibits a carbon isotopic ratio characteristic of C_4 photosynthesis (Sankhla and Ziegler, 1975), and four species—*A. glandulosa*, *A. inflata*, *A. linearis*, and *A. scoparia*—are reported to have Kranz anatomy (Lersten and Curtis,

2001). These results raise the possibility that *Anticharis* may contain both C_3 and C_4 species, and, possibly, evolutionary intermediates between the C_3 and C_4 condition. In addition, the small size of *Anticharis* indicates it may be of recent origin, and thus C_4 origins within the genus may also be recent.

To study the dynamics of C_4 evolution, it is best to examine groups with species of intermediate form. *Flaveria* (Asteraceae) best meets this criterion and has become the model group for studies of C_4 evolution (Monson and Rawsthorne, 2000; Sage, 2004; Sage *et al*., 2012). *Flaveria* has eight C_3–C_4 intermediate species, and represents the youngest known lineage of C_4 photosynthesis in the eudicots, with the C_4 pathway having arisen in the past 5 million years (Christin *et al*., 2011; R.F. Sage *et al*., 2011). As a model for C_4 evolution, however, *Flaveria* is limited in a number of ways. It lacks appreciable trait variation in the C_3 species that branch in a basal position on the *Flaveria* phylogeny (McKown and Dengler, 2007); hence initial evolutionary developments facilitating C_4 evolution cannot be readily identified (Muhaidat *et al*., 2011). It also lacks more than one C_3–C_4 intermediate species in the 'A' clade where the fully developed C_4 species occur (McKown *et al*., 2005), thereby limiting the ability to draw inferences regarding the evolutionary sequence. Most important, perhaps, is that *Flaveria* represents just one genus where the C_4 pathway arose and, hence, the universal nature of the evolutionary patterns present in *Flaveria* cannot be evaluated. To best address evolutionary lineages in complex organisms, a comparative approach must be used, whereby evolutionary trends in multiple lineages are compared (Ackerly, 1999). Ideally, lineages employed in comparative analyses would have multiple intermediate forms along an evolutionary continuum. Few C_4 lineages meet these criteria, however. Most lack C_3–C_4 intermediate species and, of those with intermediates, most have only one or two intermediate species (R.F. Sage *et al*., 2011). Few lineages have closely identified C_3 relatives, and many appear to be too ancient to retain transitional forms (Christin *et al*., 2011). Some recently studied groups show promise, notably *Cleome* (Cleomaceae; Marshall *et al*., 2007; Voznesenskaya *et al*., 2007; Feodorova *et al*., 2010) and *Heliotropium* (Boraginaceae; Muhaidat *et al*., 2011), but at best these would raise the sample size to three, which would still limit the ability to draw evolutionary inferences. There is thus great value in identifying new lineages in which to study C_4 evolution. *Anticharis* may be one such lineage.

Species of *Anticharis* grow in warm, arid regions of Africa, southern Saudi Arabia, and Southwest and South Asia (Iran, Pakistan, and India; Plant List, 2012). The phylogeny of the Scrophulariaceae places *Anticharis* in the tribe Aptosimeae, next to *Aptosimum* Burch. ex Benth. (Oxelman *et al*., 2005). At the species level, it has not been phylogenetically analysed, nor have there been detailed studies of photosynthetic pathway variation. While it is known that C_4 species are present in *Anticharis*, it is unknown whether there are C_3 species, and what relationship these may have with the C_4 species. *Anticharis* is thus one of the few lineages of C_4 photosynthesis that have not been characterized in terms of phylogeny and physiology (Muhaidat *et al*., 2007; R.F. Sage *et al*., 2011). Here, for the first time, a comprehensive analysis of the phylogeny and photosynthetic pathway distribution in *Anticharis* is presented. In addition to a carbon isotope survey and the molecular phylogeny, leaf anatomy and ultrastructure, leaf gas exchange, and the activities of the three decarboxylating enzymes were investigated in *A. glandulosa*, a C_4 species newly collected from the field.

Materials and methods

Plant material

Leaf samples of 10 *Anticharis*, one *Aptosimum*, and one *Peliostomum* species were sampled from herbarium material housed at the Royal Botanic Gardens Kew (K), the Botanische Staatssammlung München (M), and in the collection of B. Nordenstam [(Swedish Museum of Natural History (S)] (Supplementary Table S1 available at *JXB* online). Seeds of *A. glandulosa* were collected on 26 November 2005 by H. Akhani in Hormozgan Province, southern Iran, at a site 42 km SE of Minab in the direction of Senderk (26°51'36''N, 57°18'51''E; the voucher is Akhani 18314, Herb. H. Akhani). Plants were growing on dry, gravely hills with scattered shrubs at 120 m elevation (Supplementary Fig. S1). For leaf structural studies, *A. glandulosa* plants were grown from seed in 4 litre pots filled with a soil mix of 50% peat, 17% perlite, 16.5% sand, and 16.5% clay. Plants grew in a plant growth chamber (Model GC20, Biochambers, Winnepeg, MN Canada) at the University of Toronto set at a day/night temperature regime of 28 °C/20 °C, and a light intensity at the top of the plant canopy of 500 μmol photons m^{-2} s^{-1} for a 16 h photoperiod. All tissues sampled for anatomical and ultrastructural imaging were harvested in the illuminated growth chamber. For gas exchange and enzyme assays, plants were grown in a greenhouse without shade, and were supplemented with ~150 μmol photons m^{-2} s^{-1} from high pressure sodium lamps.

Anatomy and ultrastructure

Tissue was sampled for anatomical observations from recently fully expanded leaves, young stems, calyx, green immature petals, and unripe capsules of *A. glandulosa*. The internal anatomy of these tissues was assessed on 2–3 mm tissue sections prepared for light microscopy and transmission electron microscopy (TEM) as described by Sage and Williams (1995). Images of *A. glandulosa* leaf cross-sections taken at the light microscope level were used to measure leaf thickness, total cross-sectional area, percentage mesophyll (M), percentage bundle sheath (BS), and the ratio of M to BS tissue. TEM images were used to quantify chloroplast and mitochondria size as well as the density of appressed and non-appressed thylakoids (Voznesenskaya *et al*., 2007). Vein density were determined from cleared leaves of *A. glandulosa* as described by McKown and Dengler (2007). Tissues from herbarium samples were rehydrated and prepared for light microscopy (Christin *et al*., 2010) to characterize the anatomy of herbarium specimens. All quantitative measurements were made using Image J software (National Institutes of Health, Bethesda, MD, USA). Data from imaged leaf tissues of six individual plants (three leaves and 10 images per replicate) were analysed by SPSS Statistics 13.0. Normality was established using a Kolmogrov–Smirnov test, and a two-independent sample *t*-test was employed for normally distributed data, and the parameters lacking normality (including chloroplast long axis and short axis, mitochondrial area, and appressed thylakoid density) were analysed by a non-parametric Mann–Whitney U-test for two independent samples.

Immunocytochemistry

Samples embedded in London Resin White (Sage and Williams, 1995) were used for immunolocalization of Rubisco and phosphoenolpyruvate carboxylase (PEPC) as previously described (Voznesenskaya *et al*., 2007). To avoid random non-specific bindings, all sections were blocked in Tris-buffered saline–Tween-20 (TBST)+1% bovine serum albumin (BSA) (pH 7.2) for 1 h, then incubated with anti-Rubisco (diluted 1:50 in TBST), anti-PEPC (diluted 1:200 in TBST) or TBST+1% BSA as control for 3 h, and incubated again with protein A–gold 20 nm (diluted 1:100 in TBST+ BSA) for 1 h. Sections were rinsed in TBST three times after each step, then silver enhanced in the dark and observed using a

BX51 Olympus microscope. For immunolocalization of glycine decarboxylase (GDC), ultra thin silver sections, 0.4–0.6 µm, were transferred on Formvar-coated nickel grids, rehydrated in phosphate-buffered saline (PBS; 100 mM K-phosphate, 138 mM NaCl, 2.7 mM KCl, pH 7.4), blocked in PBS+4% BSA for 15 min, incubated with anti-GDC-P and anti-GDC-H (1:50 diluted in PBS+1% BSA) for 3 h, and incubated again in colloidal gold (diluted 1:20 in PBS+1% BSA) for 1 h. Sections were washed in PBS after each step, stained with uranyl acetate and lead citrate, and observed by TEM.

Gas exchange and biochemical measurements

The carbon isotope ratio ($\delta^{13}C$) was determined on ~2 mg of leaf tissue from herbarium specimens (Table 1) or fresh *A. glandulosa* using a mass spectrometer at the University of California, Davis isotope facility (http://stableisotopefacility.ucdavis.edu). Measurements of the photosynthetic response to intercellular CO_2 partial pressure (the A/C_i response) were conducted using a Li-Cor 6400 gas exchange machine (Li-Cor, Lincoln, NE, USA; Vogan *et al*., 2007). Attached leaves of greenhouse-grown plants were measured at a saturating light intensity of 1600 µmol photons m^{-2} s^{-1}, 29 ± 1 °C, and a vapour pressure deficit between leaf and air of 1–3 kPa. To contrast the A/C_i response of *A. glandulosa* with that of known C_4 and C_4-like species (Sudderth *et al*., 2007), *Flaveria bidentis* (C_4) and *Flaveria brownii* (C_4-like) were also grown in the greenhouse and the A/C_i response was measured as done for *A. glandulosa*. *Flaveria bidentis* was provided by Gerald Edwards, University of Washington; *F. brownii* was collected by R.F. Sage on Mustang Island, Texas USA in 2010.

Table 1. Results of the carbon isotope ratio ($\delta^{13}C$) for herbarium specimens

The isotope values show C_4 characteristics for the four species *A. angolensis*, *A. glandulosa*, *A. inflata*, and *A. senegalensis*.

Species	Voucher	δ13C, ‰	Photosynthetic pathway	Life form
A. angolensis	Kers 3403	–12.4	C_4	Annual
	Leistner *et al*. 109	–12.8		
A. ebracteata	Oliver, Müller & Steenkamp 6624	–25.0	C_3	Undershrub
	Giess 7864	–26.7		
	Nordenstam & Lundgren 881	–22.1		
	Nordenstam & Lundgren 810	–24.1		
A. glandulosa	Boulos *et al*. 16511	–13.7	C_4	Annual herb
	A.G.Miller & J.A.Nyberg 9447	–14.2		
	Live cotyledon grown in Toronto	–21.2[a]		
	Live leaf grown in Toronto	–17.5[a]		
	Collenette 4285	–11.1		
	Boulos *et al*. 16862	–16.8		
A. imbricata	Long & Rae 735	–27.0	C_3	Perennial undershrub
	P. G. Meyer 1148	–24.5		
	Giess, Volk & Bleissner 6212	–30.1		
	A. Engler 6062	–22.0		
	Nordenstam & Lundgren 849	–25.4		
A. inflata	Hardy & de Winter 1456	–11.7	C_4	Annual herb
	Krüger 2017	–13.1		
	Giess & Lippert 7428	–12.3		
	Nordenstam & Lundgren 2790	–12.0		
A. juncea	Dinter 5123	–21.1	C_3-C_4	Perennial-dwarf shrub
A. kaokoensis	Merxmüeller and Giess 1408	–24.9	C_3	Annual or perhaps biennial herb
A. namibensis	Nordenstam & Lundgren 380	–25.9	C_3	Annual herb
A. scoparia	Stihbauch 3756	–20.1	C3 or C3-C4	Suffruticose Perennial Herb
	Oliver, Tölken & Venter 261	–21.5		
	Merxmüller & Giess 3440	–26.1		
	Nordenstam & Lundgren 142	–24.0		
	Nordenstam & Lundgren 128	–26.5		
A. senegalensis	Collenette 4284	–15.0	C_4	Annual herb
	Harvey *et al*. 17	–13.9		
	Drummond 5690	–13.5		
	Dinter 483	–13.2		
	Winter 3421	–13.5		
	B. Hucks 1160	–13.0		
	Miller 125	–14.7		
	Nordenstam & Lundgren 319	–12.7		
	Nordenstam & Lundgren 850	–13.9		
Aptosimum indivisum	Hanekom 2017	–25.3	C_3	Perennial-dwarf shrublet
Peliostomum sp. (under *A. juncea*)	Giess 14517	–27.7	C_3	Perennial
Peliostomum viscosum E. Mey. ex Benth. (under *A.* aff. *juncea* L. Bolus)	C.A.Mannheimer & J. Mannheimer 444	–24.3	C_3	Perennial

[a]Due to a more negative source gas ratio in the Toronto air, the leaf isotope ratios are shifted to more negative values by ~2‰.

The activity of PEPCase was assayed spectrophotometrically at 340 nm by coupling production of oxaloacetic acid (OAA) to NADH oxidation using malate dehydrogenase (T.L. Sage *et al*., 2011). NAD-malic enzyme (NAD-ME) activity was measured spectrophotometrically by determining the rate of NADH formation from malate oxidation at 340 nm, and NADPH-ME activity was measured by determining the rate of NADPH formation from malate at 340 nm (T.L. Sage *et al*., 2011). The activity of PEP-caboxykinase (PEP-CK) was assayed by coupling the rate of NADH oxidation by malate dehydrogenase to the rate of OAA formation by PEP-CK (T.L. Sage *et al*., 2011).

DNA sequencing and phylogenetic analysis

DNA was extracted using an AccuPrep® GMO DNA extraction kit (Bioneer, South Korea). In this method based on the chaotropic salt, DNA binds to glass fibres fixed in a column (Carter and Milton, 1993). Amplification of the internal transcribed spacer (ITS) region (ITS1 and ITS spacers plus the 5.8S gene) used ITS5 and ITS4 primers (White *et al*., 1990) as described by Van den Berg *et al*. (2000). Amplified products were purified using an AccuPrep® PCR purification Kit (Bioneer, South Korea). Cycle sequencing reactions were performed using the BigDye Terminator Kit ver. 3.1 (Applied Biosystems, Inc., ABI, Warrington, UK) following the ABI protocols. Cycle sequencing products were cleaned using Magnesil (Promega product, Southampton, UK) on a Beckman Coulter robot (Biomek NX S8, Buckinghamshire, UK). Cleaned products were then sequenced on an ABI 3730. Sequencing output files were edited and contigs assembled using PhyDE. Sequences were first aligned automatically using Muscle (Edgar, 2004) and then edited manually following the guidelines of Kelchner (2000). The evolutionary history was inferred using maximum likelihood and 1000 replicates by MEGA5 (Tamura *et al*., 2011). The Tamura 3-parameter model with gamma rate (TN93+G) was found to fit best with an ITS data nucleotide matrix (Tamura, 1992). The tree with the highest likelihood (ln= –2747.2380) is shown (Fig. 6). Initial tree(s) for the heuristic search were obtained automatically as follows. When the number of common sites was <100 or less than a quarter of the total number of sites, the maximum parsimony (MP) method was used; otherwise the BIONJ method with the MCL distance matrix was used. The analysis involved 37 nucleotide sequences. There were a total of 696 positions in the final matrix. The MP analysis using 1000 replicates resulted in a similar topology with small differences in bootstrap supports which is not discussed herein.

Results

Carbon isotope ratios ($\delta^{13}C$ values)

In total, $\delta^{13}C$ was determined on 41 samples from 10 species of *Anticharis*, one species of *Aptosimum*, and two species of *Peliostomum* (Table 1). The *Aptosimum* and *Peliostomum* species had C_3 $\delta^{13}C$ values of –24.3‰ to –27.7‰. Four *Anticharis* species (*A. angolensis*, *A. inflata*, *A. glandulosa*, and *A. senegalensis*) exhibited C_4 $\delta^{13}C$ values ranging between –11.1‰ and –16.8‰. *Anticharis juncea* had a carbon isotope ratio of –21.1‰ that was intermediate between typical C_3 and C_4 values. Two of the five *A. scoparia* values were also in this intermediate range, although the remaining three were typical C_3 values. *Anticharis ebracteata*, *A. imbricata*, *A. kaokoensis*, and *A. namibensis* exhibited $\delta^{13}C$ values characteristic of C_3 plants or C_3–C_4 intermediate species that have little C_4 cycle activity (von Camemmerer, 1992).

Anatomy of leaves rehydrated from herbarium specimens

Leaf anatomy of the surveyed *Anticharis* species can be categorized into two main groups. The first group had a C_4 Kranz anatomy with enlarged BS cells that have a centripetal (inner) cluster of chloroplasts. The distance between each pair of vascular bundles is occupied with one or rarely two M cells. This group was made up of *A. angolensis*, *A. inflata*, *A. glandulosa*, and *A. senegalensis* (Fig. 1A–D). The second group includes five species (*A. ebracteata*, *A. imbricata*, *A. kaokoensis*, *A. namibensis*, and *A. scoparia*) that have few M cells between the vascular bundles and multiple M layers above and below the bundles (Fig. 2E–I). The BS cells are enlarged, with apparent clusters of chloroplast along the centripetal wall. Chloroplasts do not dominate the inner volume of the BS cells as they do in the C_4 leaves such as *A. glandulosa*. Vein spacing is similar to that observed in the C_4 species (Fig. 1A–D). The *Peliostomum* species (Fig. 1J) observed and *Aptosimum indivisum* have a typical C_3 leaf anatomy with several M layers on the adaxial and abaxial sides of the vascular bundles (see also Weber, 1906). The BS cells are small with little evidence of plastids. The distance between the veins is similar to that of the other *Anticharis* species.

Anatomy of Anticharis glandulosa *Asch.*

Anticharis glandulosa is an annual herb with ovate leaves ~1 × 2 cm in size (Fig. 1A). Leaves, stems, calyx, and fruits are covered by capitate glandular trichomes (Fig. 2B, 2C), while cotyledons are 2 × 3 mm in area and glabrous. The leaves, cotyledons, and calyx have a typical atriplicoid type of Kranz anatomy with centripetal chloroplasts surrounded by a single layer of M cells (Fig. 1A, 2D, 2G). Cross-sections of green stems show no evidence of Kranz anatomy in the outer cortical tissues where small plastids occur (Fig. 2E, 2F). The vascular tissue had formed a cambial layer and was initiating secondary growth. Immature petals and fruits (capsules) were green. The petals have 2–3 layers of parenchymatous M, but no evidence of Kranz tissues (Fig. 2H). Green, unripe fruits also show no Kranz-like tissues, although the mesocarp cells have many chloroplasts with large starch grains (Fig. 2I, 2J).

In leaf cross-sections, the M [photosynthetic carbon assimilation (PCA)] tissue of *A. glandulosa* covered 56% of the section while the BS [photosynthetic carbon reduction (PCR)] tissue comprised 24% (Table 2). The resulting PCA/PCR ratio was 2.5, which is typical of atriploid C_4 dicots, and well below values for C_3 species (Muhaidat *et al*., 2007). Vein density was high compared with C_3 species, and was at the upper end of C_4 dicot values (Table 2).

Transmission electron microscopy and immunolocalization

BS chloroplasts were elongated and restricted to the inner half of the BS cells, where they formed a compact mass of 2–3 ranks (Fig. 3A). Numerous large mitochondria were positioned in rows between the chloroplasts, and were generally in contact with the adjacent chloroplasts. Peroxisomes sporadically occurred on the periphery of the chloroplast matrix. The M chloroplasts were arranged around the cell periphery, but gaps were apparent between the chloroplasts and hence they do not form a continuous layer of chloroplast material facing the intercellular air spaces, as is often seen in C_3 M cell chloroplasts (Sage and Sage, 2009). Chloroplasts in the BS tissue are longer and cover more

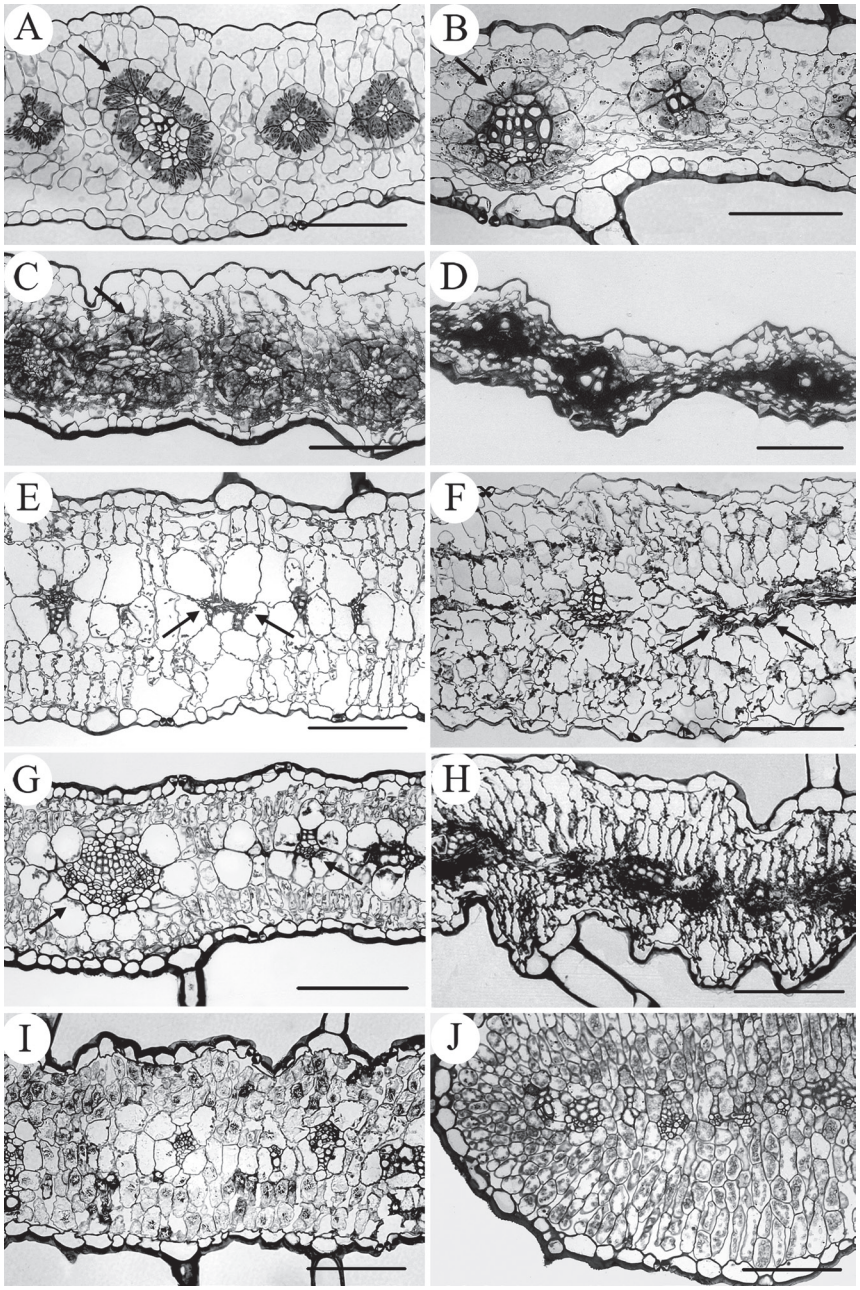

Fig. 1. Cross-sections of leaves from herbarium specimens of *Anticharis* and *Peliostomum* species (except for *A. glandulosa* which was from fresh leaves). A–D are C_4 *Anticharis* taxa, E–H are intermediate, I represents proto-Kranz, and J is C_3. (A) *Anticharis glandulosa* (cultivated, from fresh leaf material). (B) *Anticharis inflata* Giess & Lippert 7428. (C) *Anticharis senegalensis*, Nordenstam & Lundgren 850. (D) *Anticharis angolensis*, Kers 3403. (E) *Anticharis kaokoensis*, Giess & Lippert 7380. (F) *Anticharis ebracteata*, W. Giess 7864. (G) *Anticharis imbricata*, P.G. Meyer 1148. (H) *Anticharis namibensis*, Nordenstam & Lundgren 380. (I) *Anticharis scoparia*, Merxmüller & W. Giess, 3440. (J) *Peliostomum* sp., Giess *et al.* 14517). Scale bar=100 μm all panels. Arrows highlight clustered organelles along the inner bundle sheath wall.

area in section than their counterparts in the M tissues (Table 3). Mitochondria in the BS tissues are also larger than M mitochondria (Table 3). BS chloroplasts have 3–7 thylakoids per granum (Fig. 3B), while M chloroplasts have only 2–3 thylakoids per granum (Fig. 3C), thereby giving the BS chloroplasts a thylakoid index that was twice that of the M chloroplasts (Table 3).

Immunolocalizations demonstrated that the GDC-H subunit is present in the BS cell mitochondria, as indicated by the substantial binding of immunogold particles to mitochondria in the BS cells. Gold particles did not bind to mitochondria or other tissues of the M cells (Fig. 3D, 3E). Fluorescence imaging of immunolocalized antibodies to either PEPC or Rubisco demonstrated that the vast majority of PEPC expression was in the M cells (Fig. 4A), while Rubisco was mostly present in the BS chloroplasts (Fig. 4B). Notably, some label for Rubisco corresponded to M chloroplasts (Fig. 4B).

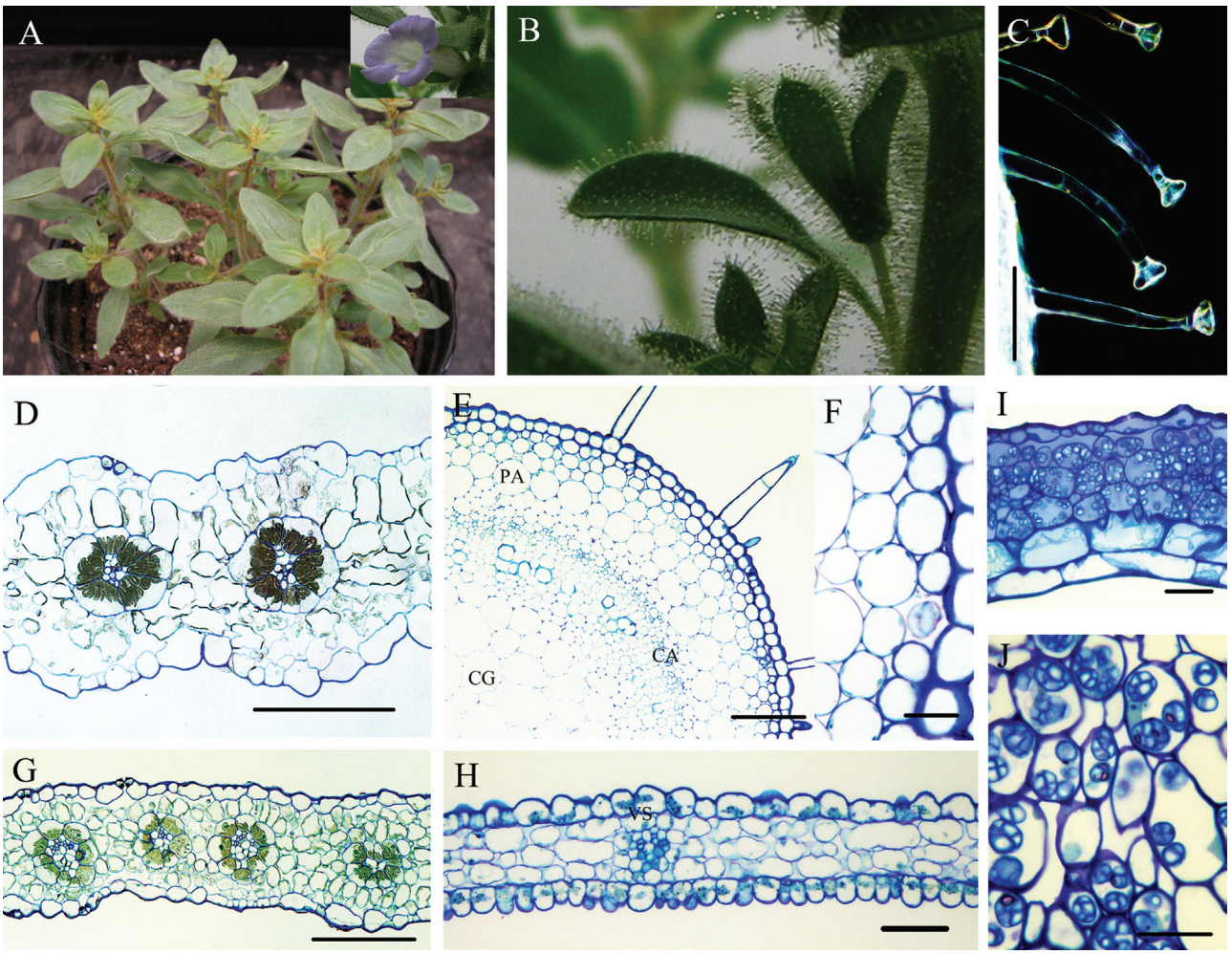

Fig. 2. *Anticharis glandulosa*. (A) A plant grown in a greenhouse. (B) Close-up of glandular trichomes covering the leaves, calyx, and stem. (C) A dark-field view of the glandular trichomes. (D) Cotyledon cross-section. (E and F) Stem cross-section. (G) Calyx cross-section with Kranz anatomy. (H) Cross-section of a petal that lacks photosynthetic parenchyma. (I) Cross-section of an immature green capsule showing exocarp, endocarp, and mesocarp layers. (J) Starch grains in the mesocarp. Pa, parenchyma; VS, vascular bundles; CA, cambium tissue; CG, central ground cells. For C, D, E, and G, the scale bar=100 μm; for H and I, the scale bar=300 μm, and for F and J, the scale bar=20 μm.

Table 2. *Values for leaf anatomical parameters of* Anticharis glandulosa *measured here from leaf cross-sections, and the same parameters measured for other species (derived from* Muhaidat *et al*., 2007)

Mean ± SD (with range), *n* = 60 for all *Anticharis glandulosa* measurements.

Variables	*Anticharis glandulosa*	Atriplicod NAD-ME dicots	Atriplicoid NADP-ME dicots	C_3 dicots
PCA[a] (M) %	56 ± 4	54.6 (12–69.2)	61.0 (44.1–74)	57.3 (36.1–84)
PCR[b] (BS) %	24 ± 3	18.3 (7.5–25.5)	16.0 (8.8–30.9)	8.1 (3.8–13.8)
PCA/PCR ratio	2.5 ± 0.1	3.1 (1.3–5)	4.4 (2.2–9.6)	11.1 (5.4–23.7)
Epidermis %	17 ± 2	18.9 (12.2–24.8)	22.8 (7.6–37.3)	14.1 (7.8–21.1)
Vein density (mm/mm^2)	13 ± 1	9.7 (6.7–14.2)	8.3 (5.4–12.4)	8.5 (4–12.4)

[a] Photosynthetic carbon assimilation cells or mesophyll cells.
[b] Photosynthetic carbon reduction cells or bundle sheath cells.

Gas exchange and enzyme assays

The response of net CO_2 assimilation rate (A) to the intercellular partial pressure of CO_2 in *A. glandulosa* showed that the CO_2 compensation point of photosynthesis was 1 μbar (Table 4). The initial slope of the A/C_i response was steep between 0 and 150 μbar CO_2, as is common in C_4 plants (Fig. 5). Above 150 μbar, there was a slight but sustained increase in A with increasing CO_2 to at least 800 μbar (Fig. 5A). There was no evidence for CO_2 saturation below 500 μbar as is apparent

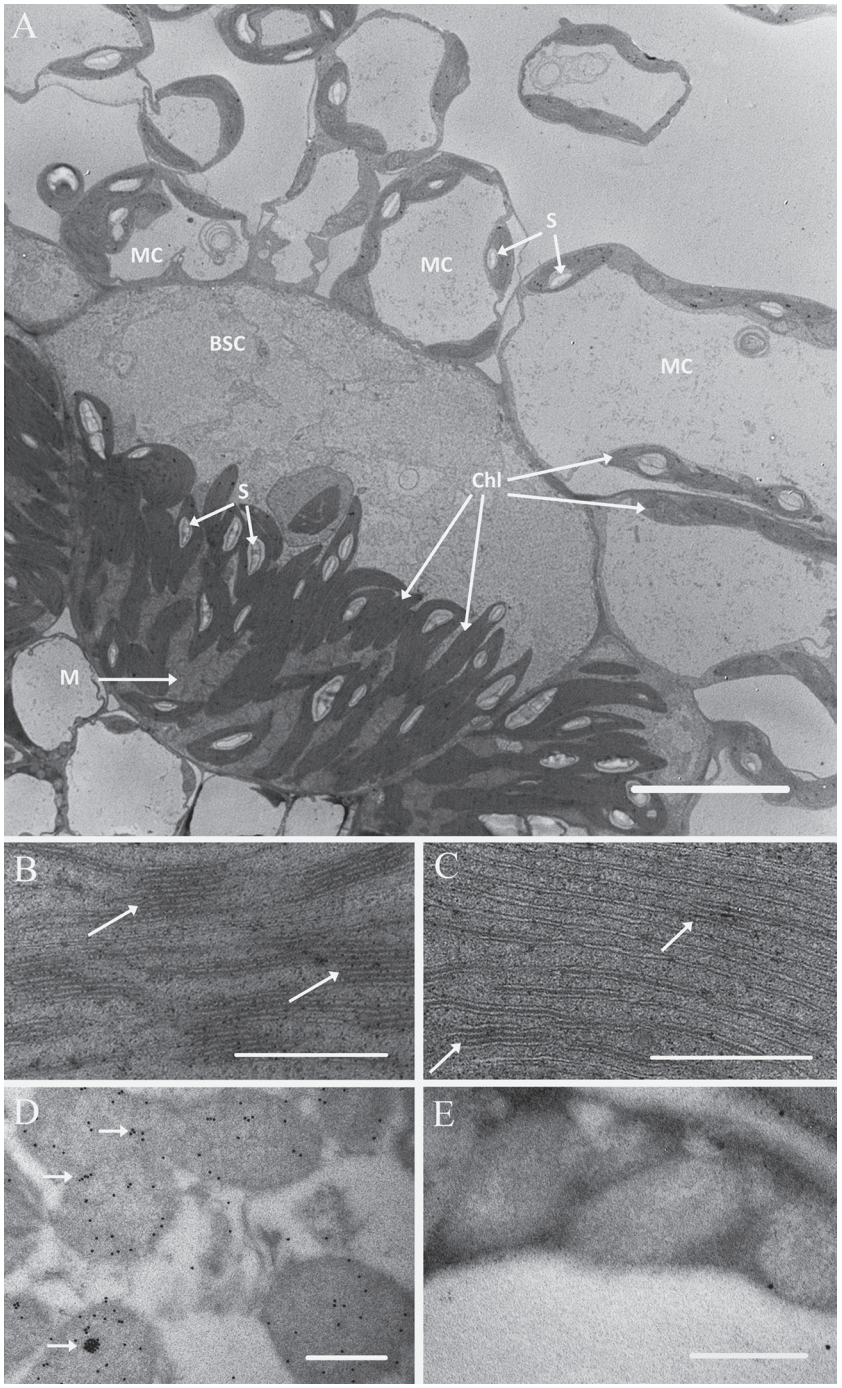

Fig. 3. (A) Transmission electron micrograph of bundle sheath cells in *A. glandulosa*. M, mitochondria; S, starch grains; Chl, chloroplast; P, peroxisome with a diagnostic crystal lattice (scale bar=10 μm). (B) Thylakoids from bundle sheath cells and (C) Mesophyll chloroplasts; arrows show appressed grana. (D) Immunolocalization of the glycine decarboxylase H subunit in bundle sheath mitochondria; arrows show specific binding of this subunit in mitochondria. (E) Mitochondria of the mesophyll cells with no specific binding of H subunit antibodies (scale bar=500 nm).

in fully developed C_4 plants such as *F. bidentis* (Fig. 5B; Edwards and Walker, 1983). In contrast, the C_4-like plant *F. brownii* also shows an upward drift in *A* with an increase in C_i above 250 μbar, although to a greater degree than in *A. glandulosa* (Fig. 5B).

The intercellular CO_2 partial pressure at current air levels of CO_2 was low (99 μbar) (Table 4), enabling *A. glandulosa* to have a high, C_4-like water use efficiency (Vogan and Sage, 2011).

Of the three C_4 decarboxylating enzymes, NAD-ME had the highest activity at 45 μmol m^{-2} s^{-1} (Table 4). This corresponded to 6 μmol min^{-1} (mg chl)$^{-1}$, which is similar to values in C_4 NAD-ME plants (Hatch *et al*., 1975; Ashton *et al*., 1990). The activity of NAD-ME was more than sufficient to maintain the

Table 3. *The size of individual chloroplasts and mitochondria, and thylakoids properties of bundle sheath and mesophyll cells from* Anticharis glandulosa

The granal index was measured as the ratio of the length of appressed grana to the length of total chloroplast grana. Thylakoid density is the total length of thylakoid membranes (in μm) per chloroplast area in μm^2. Mean ±SD. *n*=125. Sigma two tailed for independent two-samples test (for chloroplast short and long axis, mitochondria area, and appressed thylakoid density) and Mann–Whitney U-test (for the rest of the data).

Parameter	Bundle sheath cells	Mesophyll cells	Significance (two-tailed)
Chloroplast long axis (μm)	11.3 ± 4	6.9 ± 2	<0.0001
Chloroplast short axis (μm)	0.2 ± 0.05	1.8 ± 0.6	<0.0001
Chloroplast area (μm^2)	16.0 ± 5	9.0 ± 3	<0.0001
Mitochondria area (μm^2)	1. 7 ± 0.6	1.2 ± 0.5	<0.0001
Appressed thylakoid density (μm^{-1})	13.2 ± 5	5.8 ± 3	<0.0001
Non-appressed thylakoid density (μm^{-1})	23.0 ± 4	27.0 ± 6	<0.0001
Total thylakoid density (μm^{-1})	35.0 ± 6	33.4 ± 8	0.182
Granal index (%)	36.0 ± 10	18.0 ± 9	<0.0001

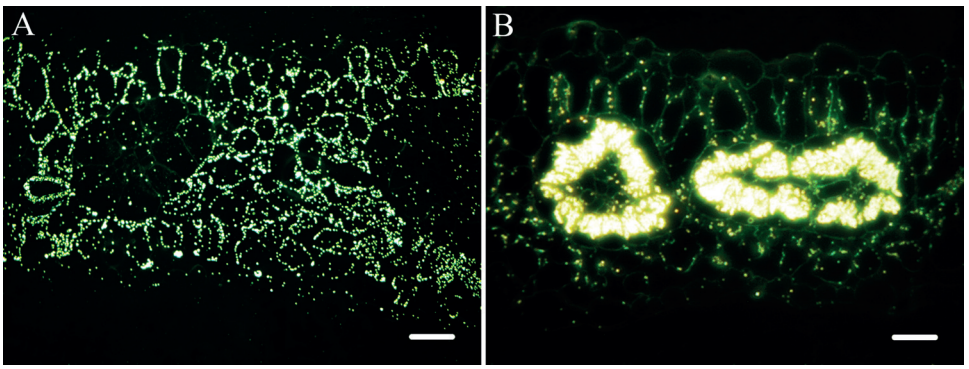

Fig. 4. Dark-field microscopy images of immunogold labelling patterns in mature leaves of *A. glandulosa*. (A) The labelling patterns of PEPC. (B) The labelling pattern of Rubisco (scale bar=30 μm).

Table 4. *Photosynthesis characteristics and activity of C_4 cycle enzymes of* Anticharis glandulosa

Means ±SD (where *n*=8) or SE (where *N*=4). For the water use efficiency (WUE) calculation, the leaf to air vapour pressure difference was standardized to 0.02 mol mol^{-1}. All gas exchange measurements were conducted at 29 ± 1 °C and light saturation. All enzyme activities were conducted at 23 °C.

Parameter	Sample size	Value	Units
Net CO_2 assimilation rate at 380 μbar	4	20.7 ± 0.9	μmol m^{-2} s^{-1}
Leaf conductance to H_2O	4	125 ± 6	mmol m^{-2} s^{-1}
Intercellular CO_2 partial pressure	4	99 ± 7	μbar
Water use efficiency	4	8.3 ± 0.3	μmol $mmol^{-1}$
Carboxylation efficiency	4	0.41 ± 0.07	μmol m^{-2} s^{-1} μbar^{-1}
CO_2 compensation point	4	1.0 ± 0.8	μbar
PEP carboxylase activity	8	149.3 ± 15.8	μmol m^{-2} s^{-1}
NADP-malic enzyme activity	8	3.0 ± 0.4	μmol m^{-2} s^{-1}
NAD-malic enzyme activity	8	44.6 ± 7.8	μmol m^{-2} s^{-1}
PEP carboxykinase activity	8	3.6 ± 1.1	μmol m^{-2} s^{-1}
Leaf chlorophyll content	8	503 ± 23	μmol m^{-2}

observed value of *A* (22.4 μmol m^{-2} s^{-1}) at air levels of CO_2. Activities of NADP-ME and PEP-CK were very low, averaging <4 μmol m^{-2} s^{-1}. PEPC activity was also high (149 μmol m^{-2} s^{-1}) and comparable with the activity seen in C_4 plants (Edwards and Walker, 1983).

Molecular phylogeny

The lengths of ITS after trimming both ends (ITS1 and ITS spacers plus the 5.8S gene) were 635–637 bp for the *Anticharis* and *Aptosimum* material, and 615 bp for the ITS from *Pelistomum*

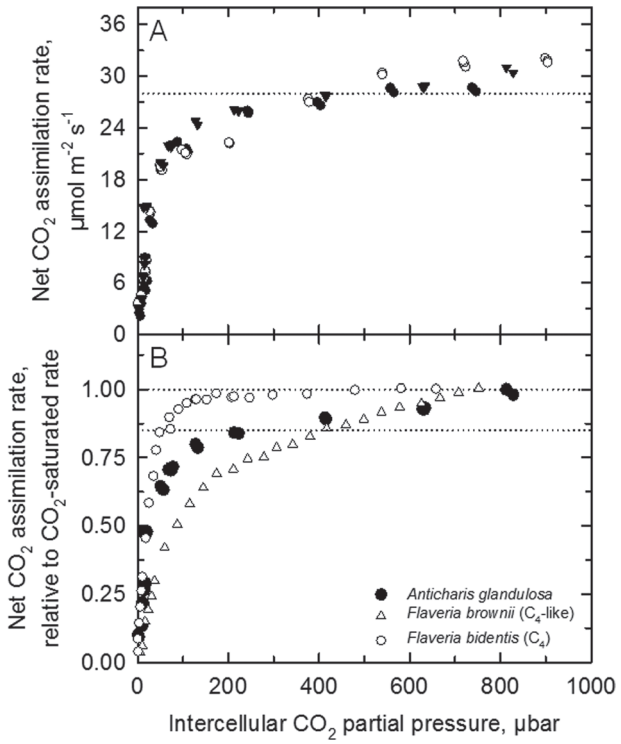

Fig. 5. (A) The response of the net CO_2 assimilation rate to variation in the intercellular partial pressure of CO_2 in *Anticharis glandulosa* at 29 ± 1 °C. Each symbol represents measurements made on a distinct leaf from one of three different plants. (B) The response of the normalized net CO_2 assimilation rate to intercellular CO_2 partial pressure in *A. glandulosa* (filled triangle, A), the C_4 plant *Flaveria bidentis* (open circles), and the C_4-like plant *Flaveria brownii* (open triangle). *A* values were normalized by dividing a given *A* by the corresponding CO_2 saturated *A*, which was 31 µmol m^{-2} s^{-1} in *A. glandulosa*, 47 µmol m^{-2} s^{-1} in *F. brownii*, and 47.5 µmol m^{-2} s^{-1} in *F. bidentis.* The presented A/C_i responses of *F. bidentis* and *F. brownii* are representative of two distinct curves.

cf. *leucorhizum*. The nucleotide percentage show higher values of G and C (31.9% and 29.9%) and lower A and T (18.7% and 19.5%). The aligned matrix contains 696 characters of which 481 sites are constant and 199 sites are variable; 131 sites are parsimony informative. The maximum likelihood search resulted in a tree of score –ln=2747.2380 (Fig. 6) that was identical in topology to the parsimony tree (not shown).

The hypothesized ITS phylogenetic tree indicates monophyly of all *Anticharis* with 99% support, and monophyly of the tribe Aptosimeae with 100% support (Fig. 6). The shrubby species *A. juncea* and *A. scoparia* branch in a basal position within *Anticharis* at a node sister to the remaining *Anticharis* species. The four species with C_4 isotopic values and Kranz anatomy (*A. senegalensis*, *A. inflata*, *A. angolensis*, and *A. glandulosa*) form a monophyletic group of annual species that branch in a distal position on the *Anticharis* tree. *Anticharis senegalensis* branches in the most basal of the C_4 species in this C_4 clade. A clade of poorly resolved species (*A. ebracteata*, *A. imbricata*, *A. kaokoensis*, and *A. namibensis*) branch between the C_4 clade and the basal clade of *A. scoparia* and *A. juncea*.

Discussion

C_4 photosynthesis in Anticharis *Endl.*

Carbon isotope ratios and the leaf anatomical survey demonstrate that four of the 10 *Anticharis* species in this study are C_4 plants. Each of these species—*A. angolensis*, *A. glandulosa*, *A. inflata*, and *A. senegalensis*—belongs to one distal clade that is apparently monophyletic, with *A. senegalensis* branching in a basal position that would indicate it is close to the original C_4 species in *Anticharis.* It should therefore be considered a priority species in follow-up studies of C_4 evolution in *Anticharis*. The *Anticharis* species branching in a basal position within the genus—*A. scoparia* and *A. juncea*—appear to be intermediate between a typical C_3 condition and a well-developed C_3–C_4 intermediate species. In *A. scoparia*, veins are closely spaced and there is no mass of plastids in the BS region of the leaf; however, BS cells are enlarged relative to the C_3 species in *Aptosimum* and *Peliostomum*, but not to the degree seen in *A. kaokoensis* and *A. imbricata*. Five leaf samples exhibited intermediate $\delta^{13}C$ values of –20.1‰ to –21.5‰, which may reflect the presence of a modest C_4 cycle or very high WUE in a C_3 plant (von Caemmerer, 1992). It was not possible to prepare a section of *A. juncea*, but it also had a $\delta^{13}C$ of –21.1‰. The clade branching between the *scoparia/juncea* branch and the C_4 clade had $\delta^{13}C$ typical of C_3 plants, but each of the species exhibited features indicative of C_3–C_4 intermediacy. In *A. ebracteata*, *A. imbricata*, and *A. kaokoensis*, vein density was high and similar to that seen in the leaf images from the C_4 species; the BS cells were enlarged to sizes similar to or exceeding the C_4 BS; and there was a mass of plastids in the BS cell. In *A. namibensis*, the vein density is also high and there is a mass of plastids apparent in the BS region of the leaves. A mass of centripetal plastids in BS cells is a general feature in C_3–C_4 intermediate plants, and it indicates the presence of a photorespiratory CO_2-concentrating mechanism variously known as glycine shuttling or C_2 photosynthesis in these species of *Anticharis* (Monson and Rawsthorne, 2000; Muhaidat *et al*., 2011; Sage *et al*., 2012).

In eudicots, C_3–C_4 intermediate species are able to concentrate CO_2 into the BS by restricting the expression of GDC to mitochondria localized along the inner wall of the BS cells (Monson and Rawsthorne, 2000). This trait forces the leaf to shuttle all glycine produced during photorespiration into the BS for metabolism by the GDC in BS mitochondria. Numerous chloroplasts form a layer alongside these inner BS mitochondria, presumably to trap and refix the photorespired CO_2 efficiently. This arrangement produces a dense aggregation of organelles along the inner wall of the BS that is readily apparent in sections from living leaves (Voznesenskaya *et al*., 2008; Muhaidat *et al*., 2011; T.L. Sage *et al*., 2011) and, as shown here, in sections of the BS cells from rehydrated herbarium leaves. If these species were indeed operating an M to BS glycine shuttle, they would probably have a C_3 $\delta^{13}C$ value, because Rubisco catalyses both the initial fixation of CO_2 in the M cells, and the refixation of photorespired CO_2 in the BS cells (von Caemmerer, 1992). For $\delta^{13}C$ to approach C_4 values, significant initial fixation via PEPC would have to occur

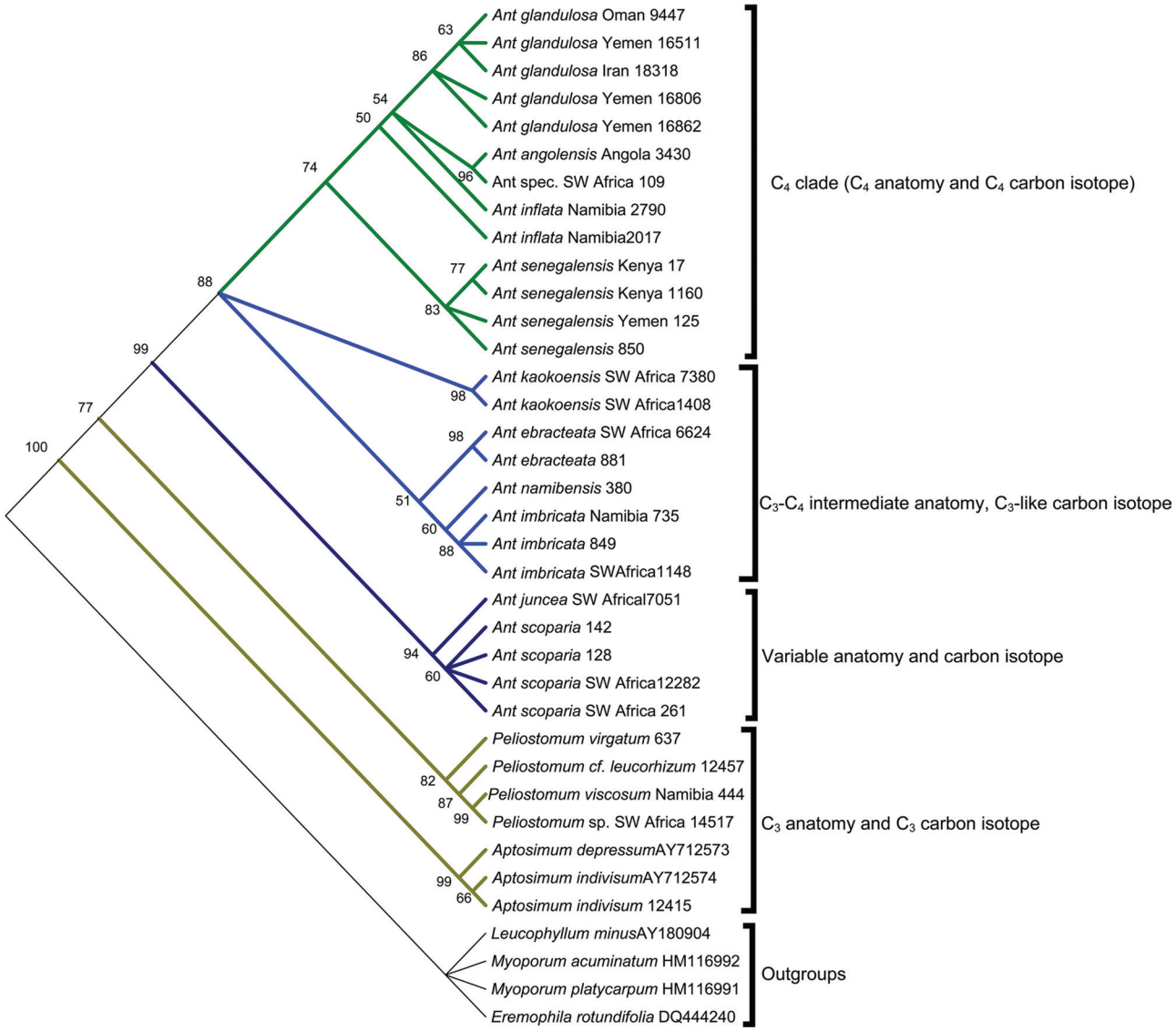

Fig. 6. A Maximum likelihood tree (ln= –2747.2380) based on ITS sequences. Numbers on nodes show maximum likelihood bootstrap support. (This figure is available in colour at *JXB* online.)

(Monson *et al*., 1988). Some C_3 species that are sister to the C_4 clades, notably in *Heliotropium* (Boraginaceae), can also exhibit enlarged BS cells, high vein density, and centripetal organelle clusters, although these do not generally approach the pattern seen in C_3–C_4 intermediates (Muhaidat *et al*., 2011). *Anticharis scoparia* is similar to these species, in that it has enlarged, but largely plastid-free BS cells that have not coalesced into a distinct wreath of cells around the vascular bundles, as have the BS cells in *A. imbricata*. The presence of incipient versions of C_3–C_4 intermediate traits in what are functionally C_3 species has been termed proto-Kranz anatomy and is proposed to represent a series of evolutionary adjustments to heat, drought, and low atmospheric CO_2, which may then facilitate the evolution of C_3–C_4 intermediacy (Muhaidat *et al*., 2011; Sage *et al*., 2012). We suggest that *A. scoparia* is a proto-Kranz species. Regardless of whether the traits observed in the non-C_4 *Anticharis* species represent full C_3–C_4 intermediacy or proto-Kranz anatomy in C_3 species, the present results present strong evidence that the species branching sister to the C_4 clade in *Anticharis* are exhibiting traits of evolutionary significance for the origin of the C_4 photosynthesis. Because all six of the non-C_4 species express traits of interest, and are phylogenetically sister to the C_4 clades, it is concluded that *Anticharis* has to be considered a potentially valuable new genus in which to study the evolutionary rise of C_4 photosynthesis.

The present study of *A. glandulosa* demonstrates that the *Anticharis* C_4 lineage is atriplicoid in terms of the C_4 anatomical type, and is the NAD-ME biochemical subtype. There is little evidence for a mixed use of decarboxylating enzymes, as NADP-ME and PEP-CK activities are low. With the addition of *Anticharis*, 43 of 62 described C_4 lineages contain species that predominantly use NAD-ME, while 21 of 36 eudicot lineages have atriplicoid Kranz anatomy.

Consistent with its being an NAD-ME type, the BS ultrastructure in *A. glandulosa* shows large numbers of mitochondria spaced between elongated chloroplasts in the inner half of the BS tissue (Miyake *et al*., 1985; Dengler and Nelson, 1999).

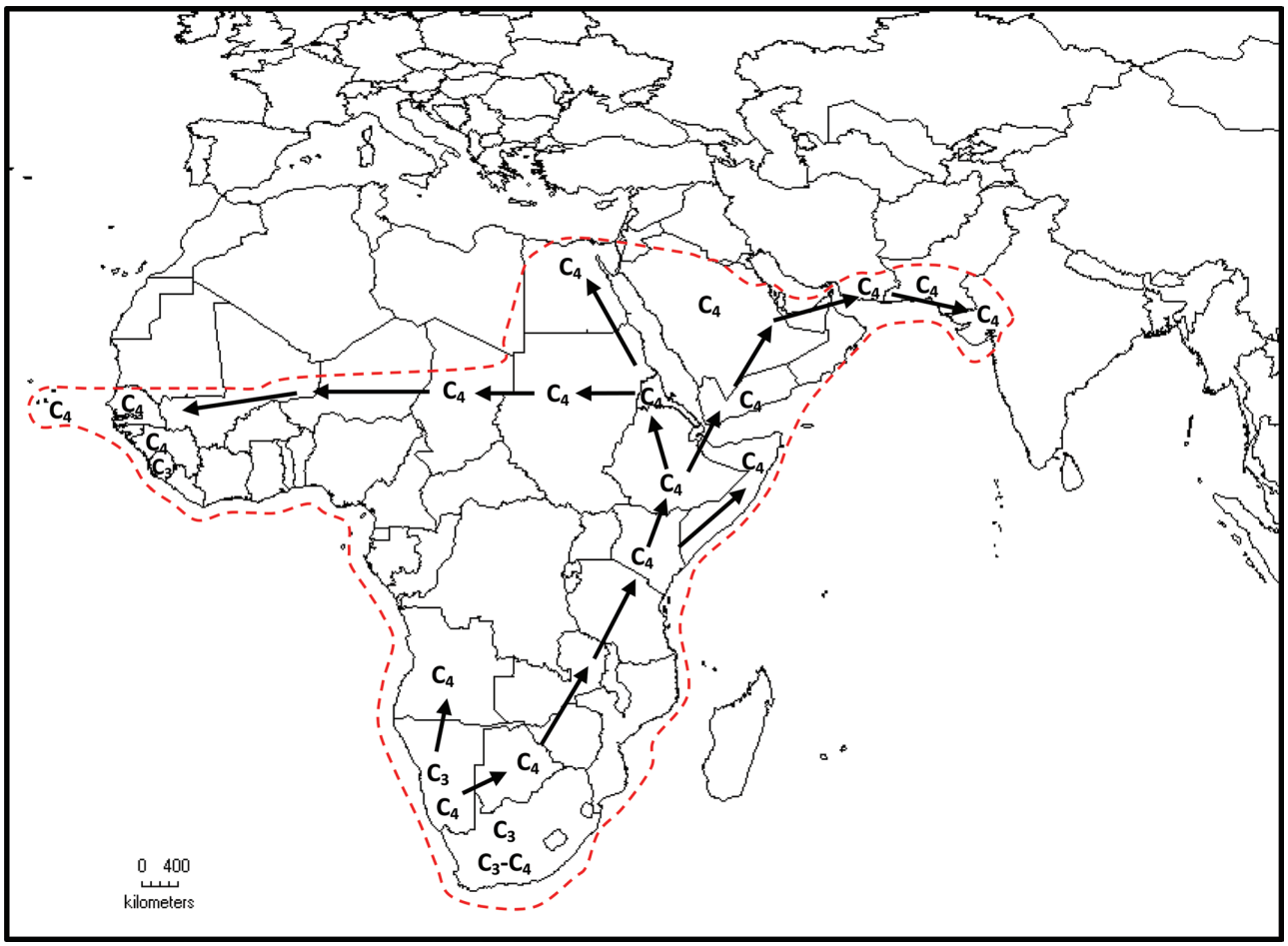

Fig. 7. The postulated centre of origin for *Anticharis* and the direction of radiation of C_4 *Anticharis* species from the centre of origin. (This figure is available in colour at *JXB* online.)

NAD-ME is a mitochondrial enzyme (Kanai and Edwards, 1999). This arrangement allows for rapid refixation of CO_2 released in the mitochondria by NAD-ME, since the close packing of mitochondria between elongated chloroplasts provides few routes of diffusive efflux for CO_2 that do not pass through an adjacent chloroplast.

In *A. glandulosa*, the chloroplasts in BS and M chloroplast are dimorphic, reflecting their optimization to their respective functions. The narrowly elongated chloroplasts in the BS would maximize surface area exposure to the adjacent mitochondria, while enlarged mitochondria are needed to metabolize rapidly four-carbon acids arriving from the M cells. This pattern is also apparent in other NAD-ME dicots such as *Atriplex rosea* (Downton *et al*., 1969), *Portulaca oleracea* (Miyake *et al*., 1985), *Blepharis ciliaris* (Akhani *et al*., 2008), and *Cleome gynandra* (Voznesenskaya *et al*., 2007). NADP-ME species, by contrast, have relatively few BS mitochondria and the chloroplasts are large and less elongated (Dengler and Nelson, 1999; Muhaidat *et al*., 2011; T.L. Sage *et al*., 2011). The granal index in *A. glandulosa* demonstrates that there is an abundance of stacked thylakoid membrane in the BS chloroplasts, which is consistent with high activity of photosystem II (PSII) and whole-chain electron transport occurring in the BS (Kanai and Edwards, 1999). NAD-ME species such as *C. gynandra* also have a high granal index in the BS relative to the M tissue (Voznesenskaya *et al*., 2007), in contrast to NADP-ME plants which have a low granal index in the BS cells (Dengler and Nelson, 1999). NADP-ME species import much of their reducing power into the BS via the C_4 metabolite malate, and thus do not need an abundance of PSII and whole-chain electron transport in BS tissues. NAD-ME species import the C_4 acid aspartate, which does not provide a net source of reducing power to the BS. Thus, they need to generate reducing power for phosphoglycerate reduction in the BS chloroplasts (Hatch, 1988; Kanai and Edwards, 1999).

The photosynthetic response to the intercellular partial pressure of CO_2 is generally consistent with the A/C_i response of C_4 plants, in that the CO_2 compensation point was near 0 µbar, the intercellular CO_2 partial pressure was less than half the ambient CO_2 partial pressure, and the initial slope of the A/C_i response was steep, allowing for relatively high rates of net CO_2 assimilation below 150 µbar. In most C_4 species, there is marked transition to CO_2 saturation below 200 µbar, and the A/C_i response above the initial slope region is flat (Sage and Pearcy, 2000). This was apparent in *F. bidentis*, a known C_4 species (Monson and Rawsthorne, 2000). In *A. glandulosa*, in contrast, there was little evidence for CO_2 saturation at low C_i, A continued to drift upwards as C_i increased above 300 µbar. *Flaveria brownii* also exhibits an A/C_i response that fails to saturate between 300 µbar

and 700 μbar. This species is a C_4-like C_3–C_4 intermediate that maintains a modest C_3 cycle in the M, and the failure of A to saturate in *F. brownii* is due to the stimulation of M Rubisco activity by elevated CO_2 (Monson *et al*., 1988; Moore *et al*., 1989; Monson and Rawsthorne, 2000). These observations indicate that *A. glandulosa* has residual C_3 cycle activity in the M, which would allow for a slight stimulation of A at elevated C_i. Immunolocalization of Rubisco further supports this possibility, since fluorescence associated with Rubisco antibodies was observed in M chloroplasts. Furthermore, the $\delta^{13}C$ values of living *A. glandulosa* which were grown were low for C_4 plants (–17.5‰ and –21.2‰), and corresponded to values seen in C_4-like plants such as *F. brownii*.

The reduction in $\delta^{13}C$ observed in the *A. glandulosa* plants was greater than the –2‰ reduction in the $\delta^{13}C$ of Toronto air relative to the bulk atmosphere, and hence would not fully explain the reductions of $\delta^{13}C$ observed in live *A. glandulosa* from typical C_4 $\delta^{13}C$ values. Some of the herbarium specimens of *A. glandulosa* had typically C_4 values, although one, Boulos *et al*. 16862, was –16.8‰, which is indicative of a C_4-like type of plant. It is hypothesized that luxurious growth conditions and a lower light intensity in the greenhouse relative to their field environments may explain the observed differences in $\delta^{13}C$. An intriguing possibility is that *A. glandulosa* expresses some M Rubisco in mild greenhouse conditions, whereas in the harsher conditions of the field it expresses fully developed C_4 photosynthesis. Similar carbon isotope behaviours have been reported in *Bienertia cycloptera*, a single-cell C_4 species that is reported to have intermediate isotope values in greenhouse-grown plants in Germany, while tissue samples collected in its native habitat of Iran show fully C_4 $\delta^{13}C$ values (Freitag and Stichler, 2002; Akhani *et al*., 2009).

Evolution and biogeography of C_4 photosynthesis in Anticharis *species*

All *Anticharis* species are arid adapted taxa and occur in the African arid belt (Jürgens, 1997). All of the non-C_4 species of *Anticharis* occur in southern Africa, with a centre of distribution in Namibia. Most of these species are perennial shrubs or woody herbs. The C_4 species, in contrast, are all annual. Of these, *A. angolensis* occurs in Angola and Namibia, *A. inflata* in Angola, Namibia, and South Africa, and *A. glandulosa* grows from NE Africa to western India. *Anticharis senegalensis* is the most widespread, being present in Angola and Namibia in south western Africa, western Africa in the Sahel region, and along the eastern parts of arid Africa from Zimbabwe to Somalia and Egypt (Supplementary Table S1 at *JXB* online). It also occurs in the southern Arabian Peninsula and across southwestern Asia to western India (Thulin, 2006). Based on the phylogeny, we hypothesize that the basal groups of *Anticharis* arose in southwestern Africa, perhaps in the Namib deserts. One of these taxa, perhaps something resembling *A. kaokoensis* or *A. imbricata*, subsequently evolved the C_4 pathway, and the resultant progeny of this origination event radiated across Africa along the arid belts, eventually reaching Southwest and South Asia, and West Africa.

These distributions provide some insights into the potential ecological drivers for C_4 evolution. The centre of distribution in Namibia is generally arid, with very hot summers and episodic rainfall events. Most rainfall occurs in summer, as part of the southern African monsoon. Summer rainfall is significant, because it allows for photosynthetic activity to be substantial during the hottest part of the year. This in turn leads to very high rates of photorespiration, which is hypothesized to be the leading physiological driver of C_4 evolution (Sage, 2004). The importance of aridity is 2-fold. First, aridity will aggravate photorespiration by preventing evaporative cooling and favouring conservative stomatal behaviour that will depress intercellular CO_2 partial pressures. Secondly, arid conditions may select for leaf anatomical traits that reduce the impact of high evapotranspiration, but may also facilitate the rise of proto-Kranz traits (Sage *et al*., 2012). In particular, aridity is proposed to select for high vein density in order to maintain a high delivery rate of water to the M tissue and thus compensate for excessive water loss in hot, low humidity environments (Sage, 2004). Once in place, high vein density may then facilitate the formation of enlarged BS cells that are more photosynthetically active, and these in turn may facilitate the origin of a glycine shuttle (Sage *et al*., 2012). With regard to these ideas, C_4-like vein densities were observed in all of the *Anticharis* species, and the fully C_3 species of both *Aptosimum* and *Peliostomum* exhibited high vein density similar to what was observed in the *Anticharis* species. This, along with similar observations in *Euphorbia* (T.L. Sage *et al*., 2011), *Heliotropium* (Muhaidat *et al*., 2011), and *Cleome* (Vosnesenskaya *et al*., 2007), implicates vein density increase as an important early event in C_4 evolution.

Conclusion

Leading models of C_4 evolution propose that C_4 photosynthesis arose from ancestral C_3 species through a stepwise acquisition of increasingly C_4-like structural and biochemical traits (Monson and Rawsthorne, 2000; Sage, 2004; Sage *et al*., 2012). *Anticharis* provides a valuable new evolutionary lineage with which to evaluate these models. It contains at least six species that are either C_3 with proto-Kranz traits, or C_3–C_4 intermediates. These species branch in the ITS phylogeny at positions that represent a series of sister nodes between the full C_3 species of *Peliostomum* and C_4 *Anticharis* species. Within *A. glandulosa*, there is evidence for Rubisco expression in the M, indicating that it expresses an initial version of C_4 photosynthesis, similar to the C_4-like species such as *F. brownii. Anticharis* is also advantageous in that it is a relatively small genus, with all of the non-C_4 species and three of the C_4 species being present in a relatively localized area of southwestern Africa. This local occurrence would facilitate the collection of live specimens and field study of nearly the entire genus. Plant biologists worldwide are encouraged to partner with Namibian colleagues to establish a living *Anticharis* collection, which could then be used for a range of studies aimed at understanding how the C_4 pathway evolved.

Supplementary data

Supplementary data are available at *JXB* online.

Figure S1. Photo from the natural habitat of *Anticharis glandulosa* in South Iran. The inset shows the dried flowering plant in October.

Table S1. List of species examined in this study with the information from the corresponding herbarium vouchers, and geographic range.

Acknowledgements

This study is part of the PhD thesis of RK and was supported by the Iran National Science Foundation (INSF) grant number 842951. A four month visit by RK to the University of Toronto was supported by an NSERC Discovery grant to RFS. We acknowledge the generous assistance of curators at the Royal Botanic Gardens Kew and Botanische Staatssammlung München with our specimen sampling, Patrick Friesen (University of Toronto) and Coresy Stinson who helped obtain the gas exchange responses, and Parastoo Mahdavi and Edith Kapinos for their assistance in the laboratory. Additional support for this study was provided to HA from the Bentham-Moxon trust and the Alexander von Humboldt Foundation while he was on sabbatical leave in the Jodrell Laboratory (Royal Botanic Gardens, Kew) and the Botanical Garden and Botanical Museum, Berlin in 2008 and 2011. Professor M. Chase (Kew) and Professor T. Borsch (Berlin) are acknowledged for their invitation and providing laboratory facilities.

References

Ackerly DD. 1999. Phylogeny and the comparative method in plant functional ecology. In: Press M**,** Scholes JD, Barker MG. eds. *Plant physiological ecology*. Oxford: Blackwell Scientific Publications, 391–413.

Akhani H, Ghasemkhani M, Chuong SDX, Edwards GE. 2008. Occurrence and forms of Kranz anatomy in photosynthetic organs and characterization of NAD-ME subtype C_4 photosynthesis in *Blepharis cilliaris* (L.) B. L. Burtt (Acanthaceae). *Journal of Experimental Botany* **59,** 1–11.

Akhani H, Lara MV, Ghasemkhani M, Ziegler H, Edwards GE. 2009. Does *Bienertia cycloptera* with the single-cell system of C_4 photosynthesis exhibit a seasonal pattern of $\delta^{13}C$ values in nature similar to co-existing C_4 Chenopodiaceae having the dual-cell (Kranz) system? *Photosynthesis Research* **99,** 23–36.

Ashton AR, Burnell JN, Furbank RT, Jenkins CLD, Hatch MD. 1990. Enzymes of C_4 photosynthesis. *Methods in Plant Biochemistry* **3,** 39–70.

Carter MJ, Milton ID. 1993. An inexpensive and simple method for DNA purifications on silica particles. *Nucleic Acids Research* **21,** 1044–1044.

Christin PA, Osborne CP, Sage RF, Arakaki M, Edwards EJ. 2011. C_4 eudicots are not younger than C_4 monocots. *Journal of Experimental Botany* **62,** 3171–3181.

Christin P-A, Sage TL, Edwards EJ, Ogburn RM, Khoshravesh R, Sage RF. 2010. Complex evolutionary transitions and the significance of C3-C4 intermediate forms of photosyntheiss in Molluginaceae. *Evolution* **65,** 643–660.

Dengler NG, Nelson T. 1999. Leaf structure and development in C_4 plants. In: Sage R**,** Monson R. eds. *C4 plant biology*. San Diego, CA: Academic Press, 133–172.

Downton WJS, Bisalputra T, Tregunna EB. 1969. Distribution and ultrastructure of chloroplasts in leaves differing in photosynthetic carbon metabolism. II. *Atriplex rosea* and *Atriplex hastata* (Chenopodiaceae). *Canadian Journal of Botany* **47,** 915–919.

Edgar RC. 2004. MUSCLE: multiple sequence alignment with high accuracy and high throughput. *Nucleic Acids Research* **32,** 1792–1797.

Edwards GE, Walker DA. 1983. *C3–C4: mechanisms, and cellular and environmental regulation, of photosynthesis*. Oxford: Blackwell.

Feodorova TA, Voznesenskaya EV, Edwards GE, Roalson EH. 2010. Biogeographic patterns of diversification and the origins of C_4 in *Cleome* (Cleomaceae). *Systematic Botany* **35,** 811–826.

Freitag H, Stichler W. 2002. *Bienertia cycloptera* Bunge ex Boiss., Chenopodiaceae, another C_4 plant without Kranz tissues. *Plant Biology* **4,** 121–131.

Hatch MD. 1988. C_4 photosynthesis: a unique blend of modified biochemistry, anatomy and ultrastructure. *Biochimica et Biophysica Acta* **895,** 81–106.

Hatch MD, Kagawa T, Craig S. 1975. Subdivision of C_4 pathway species based on differing C_4 acid decarboxylating systems and ultrastructural features. *Australian Journal of Plant Physiology* **2,** 111–128.

Jürgens, N. 1997. Floristic biodiversity and history of African arid regions. *Biodiversity and Conservation* **6,** 495–514.

Kanai R, Edwards GE. 1999. The biochemistry of C_4 photosynthesis. In: Sage R**,** Monson R. eds. *C4 plant biology*. San Diego, CA: Academic Press, 49–87.

Kelchner SA. 2000. The evolution of noncoding chloroplast DNA and its application in plant systematics. *Annals of the Missouri Botanical Gardens* **87,** 482–498.

Lersten NR, Curtis JD. 2001. Idioblasts and other unusual internal foliar secretory structures in Scrophulariaceae. *Plant Systematics and Evolution* **227,** 63–73.

Marshall DM, Muhaidat R, Brown NJ, Liu Z, Griffiths H, Sage RF, Hibberd JM. 2007. *Cleome*, a genus closely related to *Arabidopsis*, contains species spanning a developmental progression from C_3 to C_4 photosynthesis. *The Plant Journal* **51,** 886–896.

McKown AD, Dengler NG. 2007. Key innovations in the evolution of Kranz anatomy and C_4 vein pattern in *Flaveria* (Asteraceae). *American Journal of Botany* **94,** 382–399.

McKown AD, Moncalvo JM, Dengler NG. 2005. Phylogeny of *Flaveria* (Asteraceae) and inference of C_4 photosynthesis evolution. *American Journal of Botany* **92,** 1911–1928.

Miyake H, Furukawa A, Totsuka A. 1985. Structural associations between mitochondria and chloroplasts in the bundle sheath cells of *Portulaca oleracea*. *Annals of Botany* **55,** 815–817.

Monson RK, Rawsthorne S. 2000. Carbon dioxide assimilation in C_3–C_4 intermediate plants. In: Leegood RC**,** Sharkey TD, Von Caemmerer S, eds. *Photosynthesis: physiology and metabolism*. Dordrecht: Kluwer Academic Publishers, 533–550.

Monson RK, Teeri J, Ku MSB, Gurevitch J, Mets L, Dudley S. 1988. Carbon isotope discrimination by leaves of *Flaveria* species exhibiting different amounts of C_3- and C_4-cycle co-function. *Planta* **174,** 145–151.

Moore BD, Ku MSB, Edwards GE. 1989. Expression of C_4-like photosynthesis in several species of *Flaveria*. *Plant, Cell and Environment* **12,** 541–549.

Muhaidat R, Sage RF, Dengler NG. 2007. Diversity of Kranz anatomy and biochemistry in C_4 Eudicots. *American Journal of Botany* **94,** 362–381.

Muhaidat R, Sage TL, Frohlich MW, Dengler NG, Sage RF. 2011. Characterization of C_3–C_4 intermediate species in the genus *Heliotropium* L. (Boraginaceae): anatomy, ultrastructure and enzyme activity. *Plant, Cell and Environment* **34,** 1723–1736.

Oxelman B, Kornhall P, Olmstead RG, Bremer B. 2005. Further disintegration of Scrophulariaceae. *Taxon* **54,** 411–425.

Plant List. 2012. Version 1. Available at http://www.theplantlist.org/ (accessed 1 July 2012).

Sage RF. 2004. The evolution of C_4 photosynthesis. *New Phytologist* **161,** 341–370.

Sage, RF, Christin PA, Edwards EJ. 2011. The C_4 plant lineages of planet Earth. *Journal of Experimental Botany* **62,** 3155–3169.

Sage RF, Li M, Monson RK. 1999. The taxonomic distribution of C_4 photosynthesis. In: Sage RF**,** Monson RK, eds. *C4 plant biology*. San Diego, CA: Academic Press, 551–584.

Sage RF, Pearcy RW. 2000. The physiological ecology of C_4 photosynthesis. In: Leegood RC**,** Sharkey TD, Von Caemmerer S. eds. *Photosynthesis: physiology and metabolism*. Dordrecht: Kluwer Academic Publishers, 497–532.

Sage RF, Sage TL, Kocacinar F. 2012. Photorespiration and the evolution of C_4 photosynthesis. *Annual Review of Plant Biology* **63,** 1–29.

Sage TL, Sage RF. 2009. The functional anatomy of rice leaves: implications for refixation of photorespiratory CO_2 and efforts to engineer C_4 photosynthesis into rice. *Plant and Cell Physiology* **50,** 756–72.

Sage TL, Sage RF, Vogan PJ, Rahman B, Johnson DC, Oakley JC, Heckel MA. 2011. The occurrence of C_2 photosynthesis in *Euphorbia* subgenus *Chamaesyce* (Euphorbiaceae). *Journal of Experimental Botany* **62,** 3183–3195.

Sage TL, Williams EG. 1995. Structure, ultrastructure, and histochemistry of the pollen tube pathway in the milkweed *Asclepias exaltata* L. *Sexual Plant Reproduction* **8,** 257–265.

Sankhla N, Ziegler H. 1975. Eco-physiological studies on Indian arid zone plants. *Oecologia* **21,** 123–129.

Schäferhoff B, Fleischmann A, Fischer E, Albach DC, Borsch T, Heubl G, Müller KF. 2010. Towards resolving Lamiales relationships: insights from rapidly evolving chloroplast sequences. *BMC Evolutionary Biology* **10,** 352.

Sudderth EA, Muhaidat RM, McKown AD, Kocacinar F, Sage RF. 2007. Leaf anatomy, gas exchange and photosynthetic enzyme activity in *Flaveria kochiana*. *Functional Plant Biology* **34,** 118–129.

Tamura K. 1992. Estimation of the number of nucleotide substitutions when there are strong transition–transversion and G+C-content biases. *Molecular Biology and Evolution* **9,** 678–687.

Tamura K, Peterson D, Peterson N, Stecher G, Nei M, Kumar S. 2011. MEGA5: molecular evolutionary genetics analysis using maximum likelihood, evolutionary distance, and maximum parsimony methods. *Molecular Biology and Evolution* **28,** 2731–2739.

Thulin M. 2006. *Flora of Somalia* , **Vol. 3**. Kew: Royal Botanic Gardens.

Van den Berg C, Higgins WE, Dressler RL, Whitten WM, Soto Arenas, Culham MA, Chase AMW. 2000. A phylogenetic analysis of Laeliinae (Orchidaceae) based on sequence data from nuclear internal transcribed spacers (ITS) of ribosomal DNA. *Lindleyana* **15,** 96–114.

Vogan P, Frohlich M, Sage, RF. 2007. Functional signficance of C_3–C_4 intermediate traits in *Heliotropium* L. (Boraginaceae): gas exchange perspectives. *Plant, Cell and Environment* **30,** 1337–1345.

Vogan PJ, Sage RF. 2011. Water-use efficiency and nitrogen-use efficiency of C_3–C_4 intermediate species of *Flaveria Juss*. (Asteraceae). *Plant, Cell and Environment* **34,** 1415–1430.

Von Caemmerer S. 1992. Stable carbon isotope discrimination in C_3–C_4 intermediates. *Plant, Cell and Environment* **15,** 1063–1072.

Voznesenskaya EV, Akhani H, Koteyeva NK, Chuong SDX, Roalson EH, Kiirats O, Franceschi VR, Edwards GE. 2008. Structural, biochemical, and physiological characterization of photosynthesis in two C_4 subspecies of *Tecticornia indica* and the C_3 species *Tecticornia pergranulata* (Chenopodiaceae). *Journal of Experimental Botany* **59,** 1715–1734.

Voznesenskaya EV, Koteyeva NK, Chuong SDX, Ivanova AN, Barroca J, Craven LA, Edwards GE. 2007. Physiological, anatomical and biochemical characterisation of photosynthetic types in genus *Cleome* (Cleomaceae). *Functional Plant Biology* **34,** 247–267.

Weber E. 1906. Die Gattungen *Aptosimum* Burch. und *Peliostomum* E. Mey. *Mitteilungen aus dem botanischen Museum der Universität Zürich* **27,** 1–101 + Tafel I-III.

White TJ, Bruns T, Lee S, Taylor J. 1990. Amplification and direct sequencing of fungal ribosomal RNA genes for phylogenetics. In: Innis MA**,** Gelfand DH, Sninsky JJ, White TJ, eds. *PCR protocols: a guide to methods and applications*. San Diego, CA: Academic Press, 315–322.